Electro-Thermal Coupled Modeling of Induction Motor Using 2D Finite Element Method

Mustapha BOUHERAOUA[1], Mahdi ATIG[1], Amar BOUSBAINE[2], Nacereddine BENAMROUCHE[1]
[1]*Engineering Advanced Technology Laboratory (LATAGE), Mouloud Mammeri University, BP: 15000, Tizi-Ouzou, Algeria*
[2]*University of Derby, College of Engineering of Technology, Markeaton street, Derby, DE223 AW,UK*
mustapha.bouheraoua@ummto.dz

***Abstract*—The paper evaluates the thermal behavior of an induction machine based on a coupled electromagnetic-thermal model using 2D non-linear complex finite element method. The currents and the temperature distribution in a squirrel cage induction motor in transient state are investigated and presented. The convection heat transfer coefficient between the frame and ambient and the windings are treated with particular attention. The developed method can be applied to other electric machines having negligible axial heat flow. The corroboration of the theoretical/simulated results have been investigated, experimentally using a 2.2-kW totally enclosed fan-cooled induction motor. The simulated results and those obtained from measurements have been critically evaluated and showed good agreements.**

***Index Terms*—electromagnetic fields, finite element analysis, heating, induction motors, thermal analysis.**

I. INTRODUCTION

Thermal analysis has become an important step in the design and analysis of electric machines. It is used to predict the temperature rises of the critical components in order to provide sufficient optimum safety operation margins. The lumped parameter model (LPM) [1-11] and the finite element models (FEM) [12-21] are the most frequently used in thermal modeling. The LPM is based on a thermal lumped network and has been the main driver in calculating the temperature rises in electrical machines. However, it is well known that this method has some disadvantages such as it is considered to be less accurate in determining the temperature rise in the machines. It calculates only the average temperature in an active part of the motor. However, the accuracy of LPM is limited by the appropriateness of how the thermal resistance components are set and gives no detailed distribution of temperature [2-3], [17]. Convective heat transfer is still the most complex issue which needs a better understanding of fluid flow within the motor. With the increasing demand for high design accuracy, and accurate prediction of the thermal performances, it is necessary to apply the finite element method (FEM) [13-21] to model the machine structure and to predict the thermal sources as accurately as possible. The developed numerical techniques have the potential for advanced thermal designs of electrical machines especially for induction motors. The temperature distribution in the machine can be estimated and thus leading to finding the hot spots in the machine. Therefore a 2D FEM model of induction motor was used in conjunction with 3D effects for the stator and rotor circuit equations [21].The distributed heat sources are calculated using a 2D nonlinear complex finite element model (NCFEM) where the instantaneous values of currents in the stator and rotor are calculated. These thermal sources are used by the thermal model of the induction motor. The simulations were performed with the motor running at full load as this represents the state of high losses in the machine. From the local loss density distributions and the modeling of the thermal behavior in transient mode, the spatial and time dependent temperatures are derived. The convection heat exchange between the frame and the surrounding environment must be carefully modeled and evaluated. In this application, it is taken into account by the implementation of a convective exchange coefficient in the thermal program implemented under Matlab environment software.

The contribution of the paper is in addressing for the first time the convection heat transfer coefficient between the frame and the ambient. In fact to the best of our knowledge, we can state that till today no reference is available in the literature which has addressed this mater. The result is of course is an improvement of the accuracy of the electro-thermal model. This paper is organized as follows, first in section 2 we start by giving the characteristics of the studied motor. Section 3 deals with presenting in details the electromagnetic-thermal model developed. In section 4, the test rig is presented and the experimental and modeled results are compared and commented. The paper is ended by a conclusion.

II. CHARACTERISTICS OF THE CONSIDERED MACHINE

From the electromagnetic point of view, the end-effect on radial-field squirrel cage induction motor is not very important, so that a two-dimensional analysis is largely satisfactory [18], [21-22]. The three-dimensional effect is reflected by a calculation of the resistance and leakage reactance of end winding and end ring, based on analytical formulas. The analysis was performed for a 2.2-kW totally enclosed fan-cooled induction motor (TEFC) manufactured by Electro-Industries (Algeria). The geometry of the studied TEFC motor is represented in Fig. 1 and its parameters are depicted in Table I. Windings are formed of 64 conductors per slot made of a 0.75 mm diameter gauge wires.

Digital Object Identifier 10.4316/AECE.2021.02004

TABLE I. MOTOR CHARACTERISTICS

Parameters	Values
Rated power	2.2 kW
Enclosure type	TEFC
Frequency	50 Hz
Rated speed	1416 rpm
Cos φ	0.87
Rated voltage	380 V
Rated current	5.2 A
Rated Torque	15 Nm
Connection	Δ
Insulation class	F
Number of poles	4
Outer diameter of stator	145 mm
Inner diameter of stator	88.5 mm
Air-gap length	0.5 mm

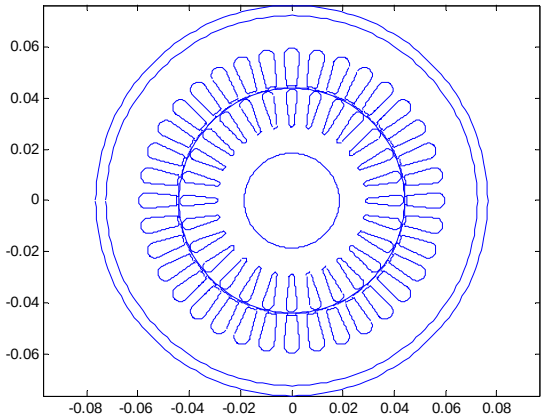

Figure 1. Cross-section of proposed induction motor

III. TWO-DIMENSIONAL FINITE-ELEMENT INDUCTION-MOTOR MODEL

A. Electromagnetic modeling of the induction motor

In this paper, a two-dimensional (2D) model is employed. The magnetic vector potential and the current density are reduced to the z components A_z and J_z respectively. Magneto dynamic complex formulation of the electromagnetic problem is used. The transient state electromagnetic equations, in: stator winding, rotor bars, air gap and outer surface have the following equations [21]:

$$curl\left(\upsilon\ curl\ (A)\right) = J \tag{1}$$

$$curl\left(\upsilon\ curl(A)\right) + \sigma\frac{\partial A}{\partial t} + \sigma GradV = 0 \tag{2}$$

$$curl\left(\upsilon\ curl\left(A\right)\right) = 0 \tag{3}$$

$$A = 0 \tag{4}$$

where:

A is the magnetic vector potential (T.m), J is the inductor current density (A/m^2), υ is the reluctivity (H^{-1}.m) and σ is the electrical conductivity (Ω^{-1}.m^{-1}).

A relation links the current density J to the vector potential A and to the electric scalar potential V:

$$J = -\sigma\frac{\partial A}{\partial t} - \sigma Grad\ V \tag{5}$$

The 2D field formulas (1) and (2) are coupled with the circuit equations of the stator windings (6) and rotor bars (7) of the machine, represented in Figs. 2 and 3 [8], [17], [23].

$$U_i = R_{ph}I_i + L_{ew}\frac{\partial I_i}{\partial t} + \frac{l}{S_C}\iint_{S_C}\beta_S\frac{\partial I_i}{\partial t}ds \tag{6}$$

$$U_i^r = R_b I_i^r + \frac{l}{S_C}\iint_{S_C}\beta_S\frac{\partial A}{\partial t}ds \tag{7}$$

where:

I_i^r is the current (A) in the bar i of section S_b (m^2) and length l (m). B_s takes into account the current direction in the slot (1 or -1) to represent forward or return paths. For the rotor bars this value is equal to 1 [21].

Field and voltage equations should be solved together as a system of equation as described in [7], [21]:

$$\begin{bmatrix} [K(A_z)] & [B_r] & [B_s] \\ [B_r]^t & [C_r] & [0] \\ [B_s]^t & 0 & [C_s] \end{bmatrix}\begin{bmatrix} [A_z] \\ [U_r] \\ [I_s] \end{bmatrix} = \begin{bmatrix} 0 \\ 0 \\ [U_s] \end{bmatrix} \tag{8}$$

where:

$[A_z]$, is the magnetic vector potential, $[I_s]$ is vector phase current and $[U_r]$ is the potential difference vector of rotor bars as unknown factors.

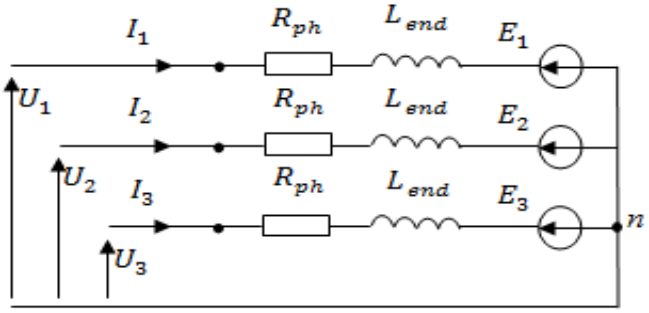

Figure 2. Stator model, R_{ph} is the stator phase resistance while L_{end} is the stator end winding inductance

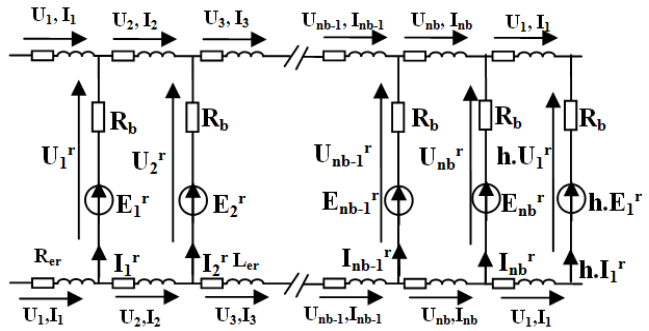

Figure 3. Rotor model, R_{er} and L_{er} are the resistance and inductance of the end ring section connecting to the cage bars R_b

Because of the nonlinearity of the core materials, Matrix [K] is non linear with respect to the vector potential $[A_z]$. Therefore the system of equations (8) must be solved using the Newton-Raphson (N-R) iteration method. The heat sources associated with magnetic field are Joule losses caused by the driving currents and the induced eddy currents. Iron losses occur in ferromagnetic materials subject to hysteresis phenomena.

B. Power losses in induction motors: heat sources modeling

It is well known that the losses generated in an induction motor are difficult to measure with an experimental technique and may be expensive and their effectiveness is often limited to specific types of motors [24]. But these values are required as the heat sources for the thermal analysis using the finite element method (FEM). If one

wants to obtain an exact and precise temperature calculation, it is, therefore, quite clear to estimate analytically or numerically power losses in the motor in order to use the estimates obtained as input parameters for thermal modeling [25]. In this analysis, these losses are initially estimated from the copper losses, the hysteresis, and the eddy current losses using the two-dimensional time harmonic finite element program using Matlab software.

From the FEM analysis, the vector potential A_z and the induced eddy current density in the rotor slots can be obtained, and the losses in the rotor bars calculated using equation (9) [21], [23].

$$P_{edy} = \frac{\overline{J} * \overline{J}^*}{\sigma_{al}} \tag{9}$$

where:

$\overline{J}^*$ is a complex conjugate of J and σ_{al} is the electrical conductivity of Aluminum.

The losses in the copper windings can, therefore, be calculated to a certain degree of accuracy using equation (10) [18], [21].

$$P_{cu1} = 3R_0\left(1+0.00393\left(T_C-25\right)\right)I_{rms}^2 \tag{10}$$

where:

R_0 is the resistance of copper at 25 °C (Ω) while T_c is the temperature of the copper winding (°C) and I_{rms} is the phase rms current (A).

The iron loss is comprised of hysteresis losses P_h, eddy current losses P_c and excess losses P_e, which can be modeled using the Bertotti-Steinmetz formula, where different coefficients are used for stator yoke, stator teeth and rotor regions [21].

$$P_{iron} = P_h + P_c + P_e \tag{11}$$

$$P_{iron} = K_h f B_m^{\beta} + K_c\left(fB_m\right)^2 + K_e\left(fB_m\right)^{1.5} \tag{12}$$

where:

K_h, K_c and K_e are loss coefficients for hysteresis, eddy current and excess losses respectively, and B_m is the peak magnetic flux density (T) and β is the Steinmetz constant, all of which depend on the lamination material. These constants can be obtained by curve fitting from manufacturer's data.

C. Electromagnetic field analysis

Electromagnetic model was used to calculate the motor losses: the copper loss of stator and rotor bars, the core loss of the stator and the rotor lamination. Fig. 4 shows the motor loss density (W/m^3) and Fig. 5 shows the flux density B distribution for a given position. This will be used to determine the iron losses in the machine given by equation 12 and the higher degree of magnetic saturation can be observed around the stator teeth.

The current density of the rotor bar is obtained through the magnetic calculation based on FEM during the full load operation.

Fig. 6 shows the flux lines distribution of the motor at no load, from which, we can see that the distribution of the magnetic field is symmetrical and the current density distribution is shown in Fig. 7 which represents the rotor Joule loss density given by equation 9. These distributions are considered as input to the thermal model analysis program. The potential differences between both ends of one rotor bar are determined using the magneto-electric coupling presented in Fig. 8.

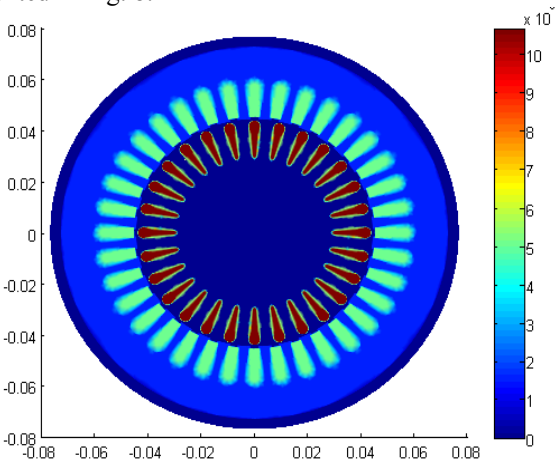

Figure 4. Loss density distribution

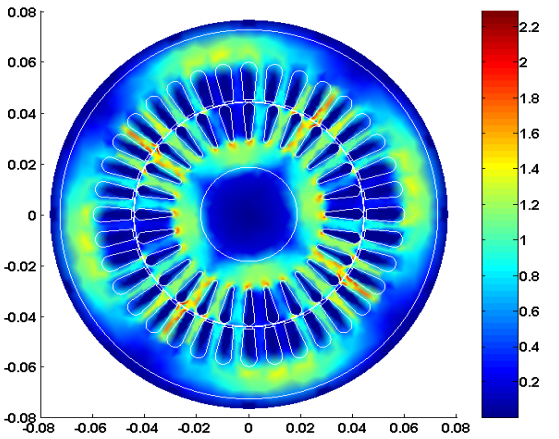

Figure 5. Flux density distribution (T)

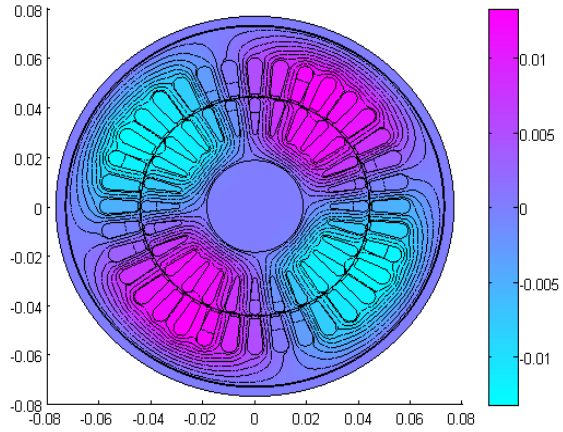

Figure 6. Flux lines of the magnetic field at no load

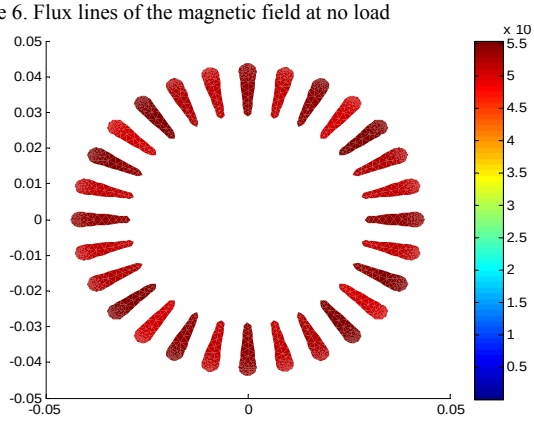

Figure 7. Current density distribution in the rotor bars (A/m^2)

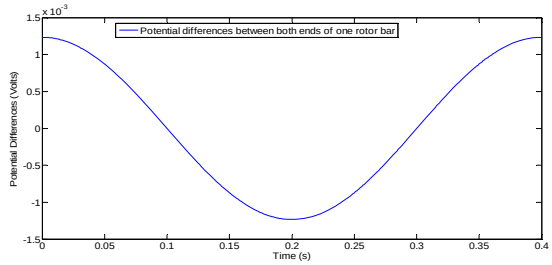

Figure 8. Potential differences in one rotor bar

D. Thermal modeling of the induction motor

For TEFC induction motor, there is no cooling system inside motor and some assumptions can be made such as: the heat flowing in the axial direction is ignored, thermal conductivity is constant over a linear element, loss density if present is also constant within an element, the temperature and loss density distribution are independent of rotor position, there is no heat flow from rotor core to the shaft, radiation heat transfer is ignored and the initial temperature was set to 25 (°C) [14], [18], [22]. Therefore, the 2D thermal analysis is well accepted for this type of motor. A contact resistance between the stator iron and the frame is taken into account [15], [22]. Heat transfer through the gap is essentially by conduction.

The 2D transient heat diffusion equation in Cartesian coordinates is given with the boundary conditions by:

$$\lambda\frac{\partial^2 T}{\partial x^2}+\lambda\frac{\partial^2 T}{\partial y^2}+q_v=\rho C\frac{\partial T}{\partial t} \tag{13}$$

where:

T is the temperature (°C), C is the heat capacity (J/°C), λ is the heat conductivity coefficient (W/m.°C), ρ is the density (Kg/m^3) and q_v is the heat sources per unit volume (W/m^3).

In the outer surface of frame, heat is mainly transferred by convection and the boundary condition is:

$$\lambda\frac{\partial T}{\partial n}+h\left(T-T_a\right)=0 \tag{14}$$

where:

h *and* h_r *are* the heat transfer coefficients (W/m^2.°C) by convection and radiation respectively, n is the vector normal to the outer surface and T_a is the ambient temperature (25 °C).

The finite element model of the heat conduction problem with mixed boundary conditions (convection, radiation) and thermal sources is given by the following matrix equation [18], [26]:

$$[K]\frac{\partial[T]}{\partial t}+[M][T]=[F] \tag{15}$$

where:

[K]: thermal capacity matrix, [M]: thermal conductivity matrix, [F]: heating sources vector.

$$M=M^e+M^\Gamma \;;\; F=F^e+F^\Gamma$$

$$K_{ij}=\rho C_p\int_\Omega N_iN_j d\Omega \;;\; M_{ij}=\lambda\iint_\Omega \nabla N_i\nabla_j d\Omega$$

$$M_{ij}^\Gamma=\left(h+h_r\right)\int_\Gamma N_iN_j d\Gamma \;;\; F_i=q_v\int_\Omega N_i d\Omega$$

$$F_i^\Gamma=\left(h+h_r\right)\int_\Gamma N_iT_a d\Gamma$$

where: N_i and N_j are the shape function.

By applying the finite difference approximations and the backward difference method, we can obtain a general equation as follow [27-28]:

$$([K]+\alpha\Delta t[M])T^{n-1}=([K]-(1-\alpha)\Delta t[M])T^n +\Delta t((1-\alpha)F^n+\alpha F^{n-1}) \tag{16}$$

Using backward difference method, we obtain:

$$\alpha_n=([K]+\Delta t[M])^{-1}\left\{F^n-[M][T^n]\right\} \tag{17}$$

$$T^n=T^{n-1}+\alpha_n\Delta t \tag{18}$$

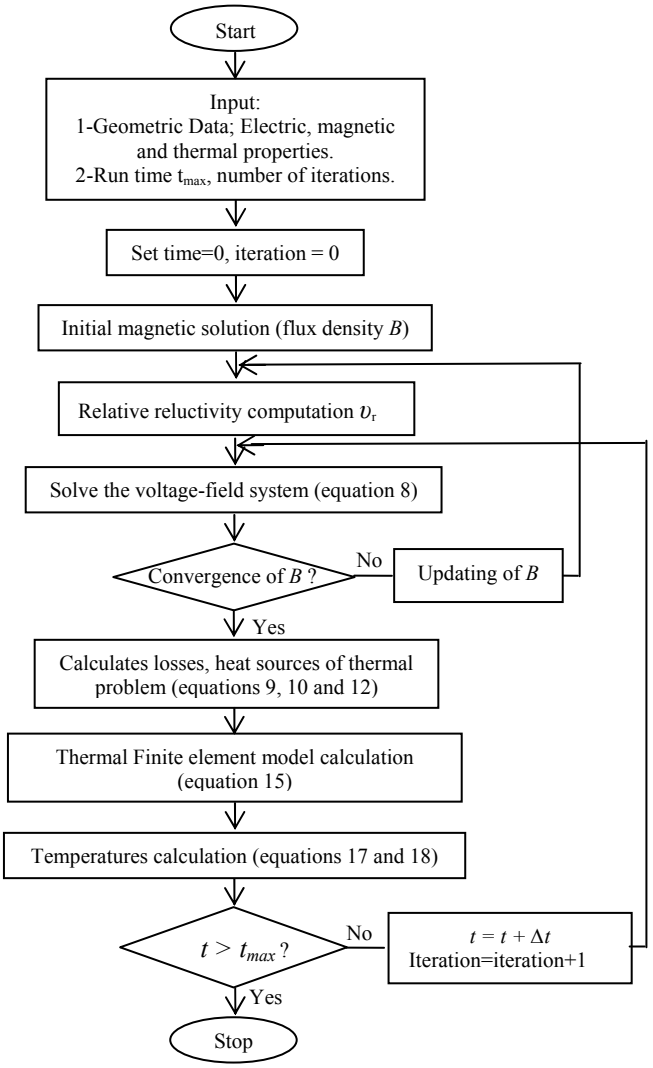

Figure 9. Coupled problem computation flow chart

The general procedure consists in solving the electromagnetic problem where the Joule and iron losses are estimated through the evolution of the stator and rotor currents as shown in Figs. 7 and 8 and the thermal problem was solved. To solve this 2D finite element problem, a program using Matlab software was developed. In the calculation of the temperature field, the heat source, heat conductivity coefficients, and heat transfer coefficients are determined based on electromagnetic and fluid analyses. The accurate calculation of these parameters is essential to obtain a realistic temperature map in the machine. In order to predict dynamic temperature distribution of the induction motor, an analysis procedure is developed and shown in Fig. 9.

E. Calculation of thermal parameters

E.1. Modeling of the air gap

The air gap problem should be specially treated when calculating the stator-rotor coupled thermal field. Because of the rotation, the air flow in the air gap is turbulent. Research in this field has shown that heat transfer in the air gap is mainly by convection. Thus the analysis of heat transfer in the air gap is very difficult and complicated. The difficulty in calculating the motor thermal field is increased greatly. In order to alleviate the problem and to simplify the calculation, the effective thermal conductivity coefficient is used and could be determined [20], [29]: Thus the rotation of the rotor and the air flow in the air gap can be assimilated as stationary and thus the heat transfer by convection is replaced by an equivalent conduction in the air gap [30].

$$\lambda_{eff} = 0.0019\eta^{-2.9084} R_e^{0.4614Ln(3.3336\eta)} \tag{19}$$

$$\eta = \frac{r_0}{R_i} \tag{20}$$

$$R_e = \omega_{\phi 1}\delta v^{-1} \tag{21}$$

where:

r_0 and R_i are respectively the stator inner diameter and rotor outer diameter (m), $\omega_{\phi 1}$ is the velocity of the rotor (m/s), δ is the length of air gap (m) and v is the cinematic viscosity of the air (m^2/s).

E.2. Modeling of the convection in the housing surface

Several empirical correlations can characterize the cooling of the external surfaces in electric machines [22], [29].

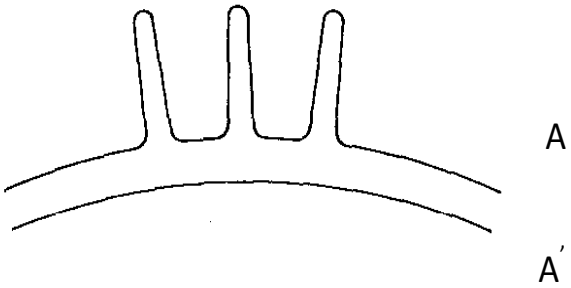

Figure 10. Fins and frame cross-section

However, the irregular geometry and the disturbed flow along the housing make its modeling difficult [22]. The realistic cross section of the frame with and without fins is shown in Fig. 10. The real surface of frame with fins is replaced by the cylindrical surface *A'* of the frame without fins having an equivalent heat transfer coefficient *h'* as:

$$h' = h\frac{A}{A'} \tag{22}$$

where:

h was calculated using the Newton's law for convection is as follow:

$$\Phi = h \cdot S\left(T_s - T_a\right) \tag{23}$$

Φ is the losses generated in the motor (W), T_s and T_a are the temperature frame surface and the ambient temperature (°C), respectively, *h* is termed the convection heat transfer coefficient ($W/m^2.°C$).

From Newton's convection law, the heat transfer convection coefficient *h* is calculated knowing the total losses Φ of the machine and the outside temperature of the frame with the ambient temperature. The outside temperature of the housing is measured experimentally with the aid of a more accurate infrared camera as shown in Fig. 11 [9].

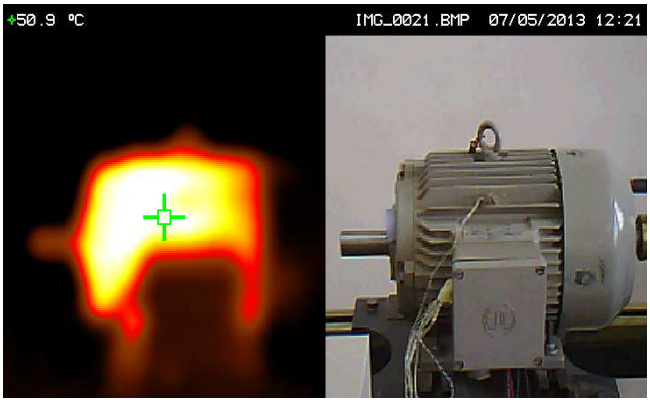

Figure 11. The frame temperature obtained by an infrared camera

The values of the thermal conductivity coefficients of the different motor regions, the heat transfer coefficient of the outer surface and the Thermo physical properties of the various components of the machine are given respectively in Table II and Table III.

TABLE II. THERMAL CONDUCTIVITIES AND FILM COEFFICIENTS USED IN THE THERMAL MODEL

Region	Thermal conductivity (W/m.°C)	Film coefficient ($W/m^2.°C$)
Frame-ambient air	-	220
Shaft (steel)	50	-
Lamination	35	-
Frame, rotor cage (aluminum)	204	-
Stator slot	0.55	-
Stator iron-frame boundary	0.023	416
Air gap	0.055	150

TABLE III. THERMOPHYSICAL PROPERTIES OF THE MACHINE

Material	$\rho(\frac{Kg}{m^3})$	$C_p(\frac{J}{Kg.C^\circ})$
Stator and rotor iron	7850	460
Slot liner	1200	1250
Housing (aluminium)	2750	940
Squirrel cage (aluminium)	2707	896
Shaft (steel)	7800	460
Copper	8933	383

E.3. Modeling of winding

The winding of the machine is a heterogeneous element of complex structure. It consists of enameled copper wires impregnated with resin that dissipate heat by the Joule effect. This component requires careful modeling, since it is the hottest point of the machine. Therefore, its thermal behavior must be reproduced as accurately as possible. The winding is considered as an equivalent homogeneous material, and the focus was on determining the values of the equivalent thermal conductivity and heat capacity. Recent work based on a four zone model using homogenization methods [18], had led to the expression (24):

$$\frac{1}{\lambda_{eq}} = \frac{\sqrt{\alpha}}{\lambda_c} + \frac{1-\sqrt{\alpha}}{\lambda_a} \tag{24}$$

where:
λ_a represents the conductivity of the air surrounding the insulated conductors of thermal conductivities λ_c and α is the fill factors of bundles conductors in a slot. The application of the various methods to our configuration gives an equivalent conductivity for the winding of 0.55 (W/m.°C) for a filling rate value of 45 %. Fig. 12 shows the evolution of the homogenized thermal conductivity of the winding and the rise in temperature as a function of the filling factor.

The temperature rise within a slot decreases with an increase of the filling factor, which shows that from thermal point of view, to increase this coefficient.

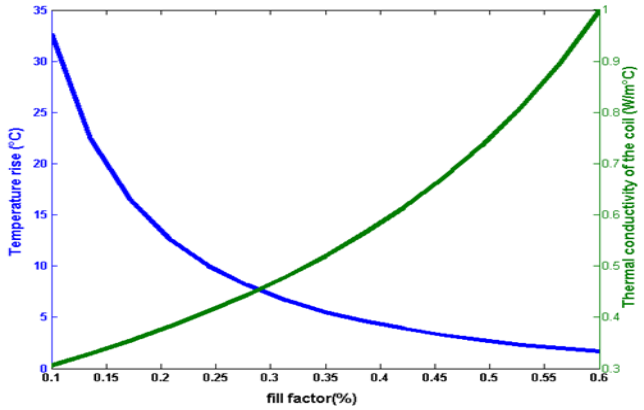

Figure 12. Evolution of the homogenized thermal conductivity of the winding and the temperature rise as a function of the filling factor in the slot

E.4. Modeling of the contact interfaces

The accuracy of motors thermal performance prediction is dependent upon the estimation of the thermal contact resistances within the machine, such as the stator lamination to housing. A contact resistance is due to imperfections in the surfaces. In fact, this is a complex function material hardness, interface pressure, smoothness of the surfaces, and air pressure [22]. In an electrical machine, there are four parts assembled which can present a thermal contact conductance: contact between rotor and shaft, contact between shaft and cap ends and roll bearings, contact between rotor bars and rotor magnetic core, contact between stator magnetic core and motor carcass.

Because of the compactness of the rotor structure (shaft, magnetic core and rotor bars) where a good thermal contact exists between laminations and squirrel cage, we take into account just the contact between stator magnetic core and motor carcass. And since the calculation is based on 2D two-dimensional FEM in radial direction, we neglected the contact between shaft and cap ends and roll bearings; the contact film coefficient h_c for stator magnetic core and motor frame is about 416 (W/m^2.°C) as shown in Table II.

E.5. Heat capacity

For homogeneous parts of the machine (carcass, rotor bar, air gap or shaft), the values of ρC_p are given either by the manufacturer or by the material data. However, it is necessary to take into account the variation of these parameters for temperature rise studies. For composite materials such as slot winding, it is necessary to calculate the properties of an equivalent homogeneous material

According to the homogenization theories, for a material composed of two elements A and B with the respective filling factors γ and 1-γ, the equivalent heat capacity is given as [18], [21]:

$$\left(\rho C_p\right)_{eq} = \gamma\left(\rho C_p\right)_A + (1-\gamma)\left(\rho C_p\right)_B \quad (25)$$

IV. Experimental Investigations and Results Analysis

In order to verify the validity of the model, a test bench has been realized. The test rig consists of a 2.2 (kW), 3-phase, squirrel-cage induction motor, mechanically coupled to a separately excited DC machine, which represents the load as shown in Fig. 13.

Figure 13. Test bench for the temperature measurement: (1) Motor, (2) DC machine, (3) Data logger, (4) Power supply

The electromagnetic field of an induction motor was analyzed by numerical method, and the distribution of current density in the cage bar at certain time could be obtained, which was shown in Fig. 7. The iron losses as well as the losses in the rotor bars are deducted which served as a source of heat in the thermal model as shown in Fig. 4. Fig. 14 shows the isothermal lines and the 2D global temperature distribution in the induction motor at rated load (s=0.05). Table IV shows the comparison between the predicted and measured steady state temperatures when the machine is on full load.

The hottest spots (120 °C) are at the rotor, we noted the considerable temperature gradient between the stator and the rotor part. The evolution of temperature in different parts of the machine is shown in Fig. 15. Our numerical calculation agrees well with our experimental result and confirms that the forced convection heat transfer coefficient between frame and ambient for the motor is nearly 220 (W/m^2.°C).

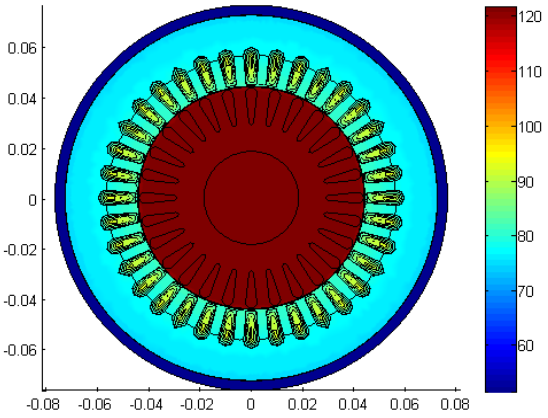

(a)

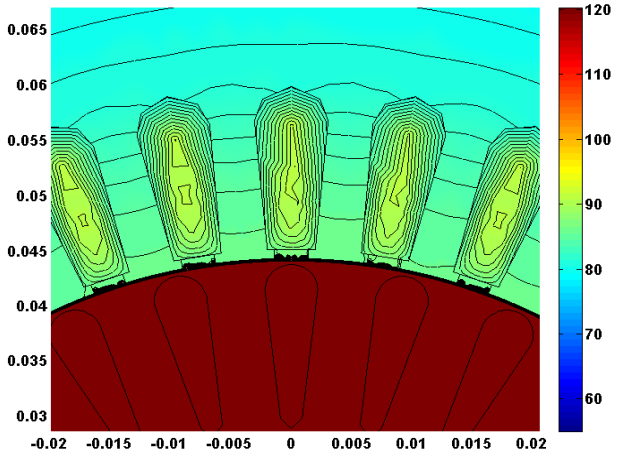

(b)

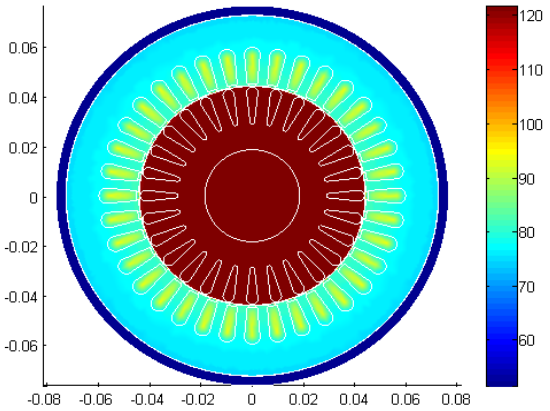

(c)

Figure 14. (a) Isothermal lines in the induction motor, (b) Zoom of field temperature at rated load, (c) Temperature distribution in the induction motor at rated load (s=0.05)

TABLE IV. COMPARISON OF MEASURED AND CALCULATED TEMPERATURES AT FULL LOAD AT STEADY STATE

Model component	Measured temperature (°C)	Finite element calculated temperature (°C)
Frame	56.56	57
Stator back iron	80.4	80
Stator teeth	89.9	90.19
Stator slot	104	103.8

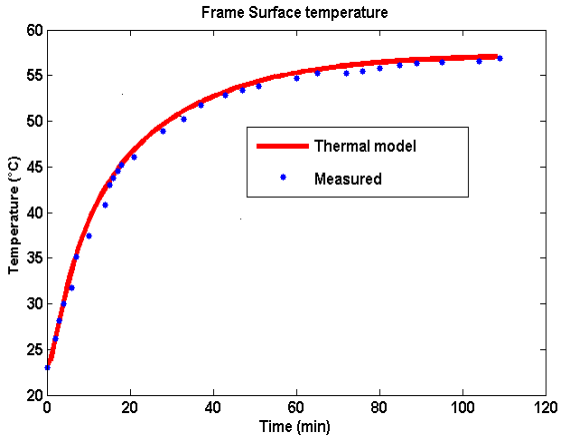

(a)

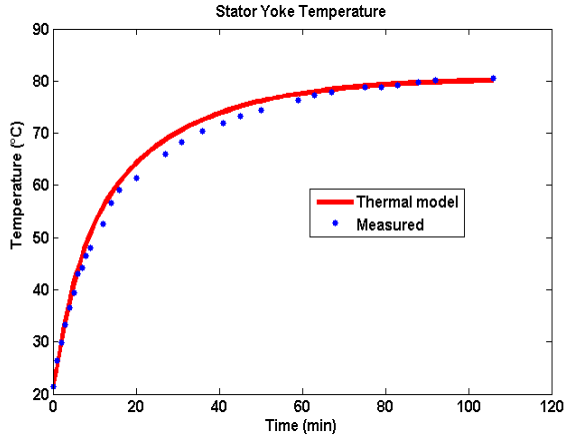

(b)

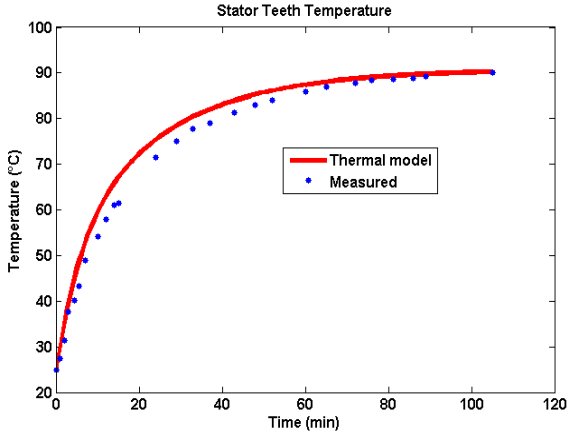

(c)

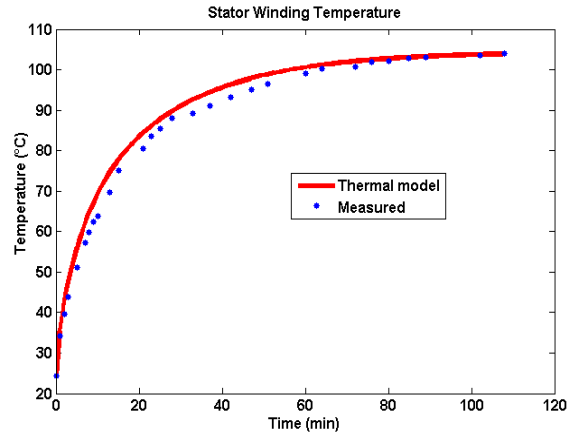

(d)

Figure 15. The temperature in different parts of the machine at rated load (a-Frame surface temperature, b-Stator yoke temperature, c-Stator teeth temperature, c-Slot winding temperature)

V. CONCLUSION

This paper presents a numerical analysis of the thermal transient behavior of an induction motor using 2D electro-thermal nonlinear complex finite element method and the 3D effect is included through the stator and rotor circuit equation under full load transient-state condition. Nonlinear complex finite element method is used to solve the electromagnetic problem and then this is coupled to the time transient thermal system. Also, in this work we introduce a new approach to take into account the convection heat transfer between the external housing and the ambient for thermal analysis. Heat transfer by convection is taken into

account by calculating the convection heat exchange coefficients in different points between the frame and the environment and introduced in the thermal model. The temperature jumps are introduced at the surfaces with a thermal contact conductance.

Results illustrate in a good manner the calculation of heat transfer coefficient by convection between frame and environment and can, therefore, be considered as the main tool in determining the temperature distribution in the motor. The results obtained by the thermal FEM model are finally validated by the experimental tests. The predicted temperatures using the coupled electro-thermal method is in close agreement with the measured ones, obtained by means of thermistor sensors of the test motor as shown in Table IV. The electromagnetic-thermal model can be extended for other motors applications.

REFERENCES

[1] Q. Chen, Z. Zou, B. CAO, "Lumped-parameter thermal network model and experimental research of interior PMSM for electric vehicle," CES Transactions on Electrical Machines and Systems, pp. 367-374, December 2017. doi:10.23919/TEMS.2017.8241358

[2] A. Adouni, A. J. M. Cardoso, "Thermal analysis of synchronous reluctance machines–a review," Electric Power Components and Systems, pp. 1-15, April 2019. doi:10.1080/15325008.2019.1602688

[3] Y. Ebrahimi, M. R. Feyzi, "Lumped parameter thermal model for axial flux switched reluctance motors," Electric Power Components and Systems, pp. 2318-2326, May 2017. doi:10.1080/15325008.2017.1333545

[4] P. S. Ghahfarokhi, A. Kallaste, A. Belahcen, T. Vaimann, A. Rassõlkin, "Hybrid thermal model of a synchronous reluctance machine," Case Studies in Thermal Engineering, pp. 381-389, September 2018. doi:10.1016/j.csite.2018.05.007

[5] Y. Yang, B. Bilgin, M. Kasprzak, S. Nalakath, H. Sadek, M. Preindl, A. Emadi, "Thermal management of electric machines," IET Electrical Systems in Transportation, pp. 104-116, June 2016. doi:10.1049/iet-est.2015.0050

[6] C. Sciascera, P. Giangrande, L. Papini, C. Gerada, M. Galea, "Analytical thermal model for fast stator winding temperature prediction," IEEE Transactions on Industrial Electronics, pp. 6116-6126, August 2017. doi:10.1109/TIE.2017.2682010

[7] M. Bouheraoua, N. benamrouche, A. Bousbaine, "A more refined thermal model for a totally enclosed fan-cooled induction motor," Electric Power Components And Systems, pp.179-194, October 2011. doi:10.1080/15325008.2011.629334

[8] N. Benamrouche, M. Bouheraoua, S. Haddad, "A thermal model for a TEFC induction motor-development and sensitivity analysis," Elect. Power Component And Systems, pp. 259–269, 2006. doi:10.1080/15325000500240862

[9] R. Khaldi, N. Benamrouche, M. Bouheraoua, "Experimental identification of the equivalent conductive resistance of a thermal elementary model of an induction machine," American Journal of Electrical Power and Energy Systems, pp.15-20, March 2014. doi:10.11648/j.epes.20140302.11

[10] M. Atig, M. Bouheraoua, R. Khaldi, "Thermal study of three-phase squirrel cage induction motor with the open-phase fault operation using a lumped parameter network (LPTN)," European Journal of Electrical Engineering, pp. 87-94, April 2021. doi:10.18280/ejee.230201

[11] P. H. Mellor, D. Roberts, D.R. Turner, "Lumped parameter thermal model for electrical machines of TEFC design," IEE Proceedings-B, pp. 205-218, September 1991. doi:10.1049/ip-b.1991.0025

[12] D. Joo, J. H. Cho, K. Woo, B. T. Kim, D. K. Kim, "Electromagnetic field and thermal linked analysis of interior permanent-magnet synchronous motor for agricultural electric vehicle," IEEE Transactions on Magnetics, pp. 4242-4245, September 2011. doi:10.1109/TMAG.2011.2149504

[13] D. G, Nair, P. Rasilo, A. Arkkio, "Sensitivity analysis of inverse thermal modeling to determine power losses in electrical machines," IEEE Transactions on Magnetics, pp. 1-5, July 2018. doi:10.1109/TMAG.2018.2853084

[14] S. Mezani, N. Takorabet, B. Laporte, "A combined electromagnetic and thermal analysis of inductions motors," IEEE Transactions on Magnetics, pp. 360–372, May 2005. doi:10.1109/TMAG.2005.845044

[15] J. Driesen, R. J. M. Belmans, K. Hameyer, "Finite element modelling of thermal contact resistances and insulation layers in electrical machines," IEEE Transactions on Magnetics, pp. 15-20, February 2001. doi:10.1109/28.903121

[16] J. Driesen, R. Belmans, K. Hameyer, "Coupled magneto-thermal simulation of thermally anisotropic electrical machines," IEEE International Electric Machines and Drives Conference. IEMDC'99 Proceedings (Cat. No. 99EX272), pp. 469-471, May 1999. doi:10.1109/IEMDC.1999.769149

[17] Y. C. Chong, "Thermal analysis and air flow modelling of electrical machines," Doctoral dissertation, University of Edinburgh, Edinburgh, UK, 2015

[18] E. Chauveau, Contribution au calcul électromagnétique et thermique des machines électriques. Application à l'étude de l'influence des harmoniques sur l'échauffement des moteurs asynchrones. Doctoral dissertation, University of Nantes, France, Novembre 2001

[19] J. H. Lee, A. R. Jeon, "Heat characteristics analysis of synchronous reluctance motor using FEM coupled electromagnetic field and thermal field," Journal of Magnetics, pp. 138-142, September 2010. doi:10.4283/JMAG.2010.15.3.138

[20] N. Bianchi, Electrical machine analysis using finite elements, 1st Edition, Taylor & Francis Group, USA, 2005

[21] A. Arkkio, "Analysis of induction motors based on the numerical solution of the magnetic field and circuit equations," Doctoral dissertation, Helsinki University of Technology, Finland, December1987

[22] A.Bousbaine, "An investigation into thermal modelling of induction motors," Doctoral dissertation, The University of Sheffield, U.K, 1993

[23] G. Bertotti, A. Boglietti, M. Chiampi, D. Chiarabaglio, F.Fiorillo, M. Lazzari, "An improved estimation of iron losses in rotating electrical machines," IEEE Transactions on Magnetics, pp. 5007-5009, November 1991. doi:10.1109/20.278722

[24] A. Mihalcea, B. Szabados, J. Hoolboom, "Determining total losses and temperature rise in induction motors using equivalent loading methods," IEEE transactions on Energy Conversion, pp. 214-219, 2001. doi:10.1109/60.937199

[25] A. Bousbaine, "Thermal modelling of induction motors based on accurate loss density distribution," Electric Machines & Power Systems, pp. 311–324, 1999. doi:10.1080/073135699269325

[26] Y. Liu, Y. Lee, H. K. Jung, S. Y. Hahn, J. H. Youn, K. W. Kim, J. I. Lee, "3D thermal stress analysis of the rotor of an induction motor," IEEE Transactions on Magnetics, pp. 1394-1397, July 2000. doi:10.1109/20.877699

[27] L .J. Segrlind, Applied finite element analysis, 2nd Edition, John Wiley & Sons, 1984

[28] C. C. Hwang, C. T. Pan, "Comparison of finite element methods for the diffusion problem," International Journal of Systems Science, pp. 1165-1179, 1988. doi: 10.1080/00207728808547153

[29] F. Incropera, "Fundamentals of heat and mass transfer," Third Edition, John Wiley & Sons, 1990

[30] C. Mademlis, N. Margaris, J. Xipteras, "Magnetic and thermal performance of a synchronous motor under loss minimization control," IEEE transactions on Energy Conversion, pp. 135–142, June 2000. doi:10.1109/60.866990